Metaplasticity and Continual Learning: Mechanisms subserving Brain Computer Interface Proficiency

Shuo-Yen Chueh[1], Yuanxin Chen[1], Narayan Subramanian[1], Benjamin Goolsby[2], Phillip Navarro[1], Karim Oweiss[1,2,3,4,*]

[1]Department of Electrical and Computer Engineering,[2]Department of Biomedical Engineering,[3]Department of Neuroscience,[4]Department of Neurology
University of Florida, United States of America

*Corresponding Author: koweiss@ufl.edu

Abstract

Objective: Brain Computer Interfaces (BCIs) require substantial cognitive flexibility to optimize control performance across diverse settings. Remarkably, learning this control is rapid, suggesting it might be mediated by neuroplasticity mechanisms operating on very short time scales. However, these mechanisms remain far from understood. Here, we propose a metaplasticity model of BCI learning and skill consolidation at the single cell and population levels comprised of three elements: a) behavioral time scale synaptic plasticity (BTSP), b) intrinsic plasticity (IP) and c) synaptic scaling (SS) operating at time scales from seconds to minutes to hours and days. Notably, the model is able to explain *representational drift* – a frequent and widespread phenomenon observed in multiple brain areas that adversely affects BCI control and continued use.

Approach: We systematically characterized plasticity induced in single neurons using two photon optogenetics. We further quantified learning progression in mice learning BCI control both within session (seconds to minutes) and across multiple sessions (days and weeks).

Main results: We found that on the time scale of seconds to minutes, substantial BTSP could be induced and was associated with significant IP. Over the time scale of days and weeks, these changes could accurately predict BCI control proficiency, suggesting that synaptic scaling may complement both BTSP and IP to stabilize and consolidate BCI control.

Significance: Our results provide theoretical and early experimental support for an integrated metaplasticity model of continual BCI learning. The model's predictions may be used to design and calibrate neural decoders with complete autonomy while considering the temporal and spatial scales of plasticity mechanisms and their anticipated order of occurrence. With the power of modern-day machine learning (ML) and artificial Intelligence (AI), fully autonomous neural decoding and adaptation in BCIs might be achieved with minimal to no human intervention.

MAIN

Implantable BCI technology have made striking advances over the last two decades, with numerous proofs of concept for rapid and efficient neural control of prosthetic and communication devices by neurologically impaired subjects [1-6]. At the heart of these advances are two important principles. The first principle is the neural decoder design which involves real time mapping of neural activity patterns to control signals that drive an agent in the task space– refered to as exogenous BCIs[7] (e.g. a computer cursor or a multi degree of freedom (DOF) prosthetic limb[2,3]). It could also involve directly stimulating neurons based on decoded neural activity patterns to achieve a desirable functional outcome, such as inducing Hebbian plasticity between recorded and target brain regions[10] (refered to as endogenous BCIs [7]). The second principle, which is a distinguishing feature of exogenous BCIs, involves the availability of natural sensory feedback once the BCI loop is closed; it allows the subject to learn which neural activity patterns are rewarded and hence should continue to be reinforced. It is believed that neuromodulatory signals play a key role in this process, both at the single cell level as well as the population levels, allowing subjects to optimize BCI performance with repeated practice[8,9] as in natural motor skill learning.

A notable observation in BCI studies, however, is the speed of learning, which can be in the order of a few minutes per degree of freedom [10-14], although this depends on the training paradigm[15-17] and the decoder design[18,19]. This is in sharp contrast to natural motor skill learning which takes many hours and days of practice. Early work suggested that the standard Hebbian synaptic plasticity—resulting from (nearly) coincident depolarization of pre- and postsynaptic neurons—could be a biologically plausible mechanism that underlie this rapid learning [20,21,9]. However, the most documented forms of Hebbian plasticity occur on the time scale of a few milliseconds[22-26], which is insufficient to incorporate sensory feedback – an indispensable component in BCI learning, which is in the order of few tens of milliseconds[27]. Furthermore, co-activation of pre- and postsynaptic activity at larger intervals (seconds or longer) is known to produce no synaptic plasticity [28,29]. More recent work suggested that dopamine D1 receptor (D1R) activation in the striatum within 500 ms was sufficient to drive reinforcement of preceding cortical patterns. Crucially, this reinforcement was cumulative, time dependent and was independent of a behavioral outcome or a reward.

Aside from plausible mechanisms of BCI learning, another notable observation in both BCI and non-BCI studies is the occurrence of *representational drift* [30-35] – defined as a consistent shift in the representation of decoded variables despite that the associated behavioral and environmental conditions remain unchanged[31,36]. In BCI settings, this necessitates frequent decoder calibration and possible corrective approaches to misclassified/missing data [8,37-39]. Together, these observations and the lack of understanding of their underlying causes during continued BCI use have been a major impediment to BCI large scale translation with full autonomy[40].

Herein, we propose a mechanistic model involving the integration of multiple distinct forms of plasticity spanning different time scales that are consistent with the above observations (Figure 1). The model comprises three elements: behavioral time scale synaptic plasticity (BTSP), intrisinc plasticity (IP) and synaptic scaling (SS). First, we posit that the primary mechanism for fast learning within the first few BCI trials is mediated by BTSP taking place over a few seconds to minutes [41-44], consistent with a neuromodulatory effect involving D1R activation within a sub-

second timescale [45]. Second, we posit that the re-occurrence of rewarded activity patterns triggers IP over relatively longer time scales within minutes to hours. This process, in turn, results in perturbation of the homeostatic state of the circuits within which BCI neurons are embedded. The ensuing imbalance of excitation/inhibition (E/I) within these circuits triggers a restoration of an E/I balance through synaptic scaling[46,47], a much slower process that operate over time scales of days and possibly weeks. We posit that the interaction between these three elements reconciles multiple findings and provides a more accurate account for BCI learning, skill consolidation, and practical implementation during everyday use.

Figure 1 Metaplasticity model for BCI learning and continued use

Rapid BCI learning and Behavioral Time Scale Synaptic Plasticity

BTSP is a short-term, non-Hebbian plasticity mechanism that is distinct from Long Term Potentiation (LTP), Long Term Depression (LTD) or Spike Timing Dependent Plasticity (STDP), in which presynaptic activity alters synaptic efficacies over behaviorally relevant time scale (seconds)[41,48]. It has been first demonstrated in hippocampal area CA1 neurons *in vivo* within a handful of trials during place cell formation [41,48,49]. The basic idea is that presynaptic inputs that were neither causal nor close in time to postsynaptic activation can be potentiated if dendritic Ca^{2+} 'plateau potentials' are present around the dendritic structure where these inputs were received. These plateau potentials are generated by complex spiking and cause an increase in the weights of excitatory inputs from presynaptic neurons, essentially creating the so called 'eligibility trace' that interacts with an instructive signal (e.g. a reward input) to determine which synapses to potentiate. Most strikingly, the magnitude of this potentiation permits this phenomenon to occur without substantial repetition (1.4 trials under natural place field input, 5.1 trials under induced place fields in the hippocampus [31]). A learning rule responsible for input potentiation would therefore span a much longer time (seconds) than predicted by standard Hebbian rules (tens of milliseconds) to include inputs that were not directly involved in driving neuronal firing. The dynamics of this process are strikingly similar to the time scale governing dendritic spine enlargement by glutamate uncaging followed by dopaminergic input within 0.3 to 2 seconds [45].

It has been consistently observed that the agent control during the first few BCI trials is slow and relies crucially on sensory (mostly visual) feedback to make instant corrections to the BCI controlled variable(s). In the non-biomimetic approach to BCIs in which an arbitrary decoder is built without knowledge of the functional tuning of BCI neurons [18,50], neural activity has been characterized during the first few trials by complex spiking patterns [11,12], with variations spanning a few seconds, suggesting 'a search' could be taking place in the neural state space for an optimal neural spiking patterns to drive the decoder [51]. This search would involve finding an optimal input to these neurons to evoke these patterns that maximize the decoder's output in a statistical sense. It is therefore conceivable that, instead of multiple pre and post synaptic spike pairings within tens of milliseconds (as the standard Hebbian SP would require), an optimal input to BCI neurons would produce a single Ca^{2+} plateau potential in dendrites that last for tens of seconds [44]. Dopamine release over a comparable time scale would therefore be sufficient to reinforce afferent sensory feedback information at selected dendritic spines, which would typically arrive tens of milliseconds later [27,52, ,53]. These inputs arriving at different times would then be

potentiated if they are most relevant to the agent's rewarded behavior. Specifically, the delayed, stochastic nature of these synaptic inputs would correspond to different error magnitudes in the task space, some would be small during trial epochs in which the agent's evolving trajectory approaches the target (hence reward predicting[54,55]), while others would be large around epochs in which the agent is moving away from the target. As such, past synaptic inputs from co-active, presynaptic neurons and postsynaptic activation by dendritic plateaus facilitated by local dopamine release would alleviate the need for instant correlation of neurons controlling the BCI, and this would be sufficient to induce tuning of BCI neurons to the decoded variable(s) in very few trials consistent with a BTSP rule. An important metric to support this model would be evidence that a rapid transition from failed trials early in the training session to successful trials later in the session is a good predictor of an overall high performance both within the remainder of the first session as well as across sessions.

Representational Drift and BCI decoder calibration

While BTSP could explain the rapid and flexible control associated with early BCI learning, it cannot explain the need for frequent decoder calibration over behavioral sessions [8,19]. This calibration is intended to deal with uncontrolled changes in signal quality and information content that are typically observed over the slower time scales of days and weeks [56]. These can be broadly categorized as: 1) degradation in signal quality that are associated with specific events such as neuronal displacement and glial reaction to device implantation which typically occurs within the hours and days following the event (but could persist over longer periods) [57-59] and, 2) shifts in information content in the form of changes in firing statistics despite that the associated behavioral and environmental conditions remain unchanged[31,36]. This representational drift has been observed in sensory and association areas of cortex as well as the hippocampus [32-35], and is not specific to electrical recording methods but have also been observed with optical imaging methods. It takes place at constant rates after a task has been learned and is substantially different from those associated with specific events [30,31]. Most strikingly, drift rate in the same subject can differ across contexts, suggesting it may be a function of the behavior performed during the period of observation[60]. Recent computational modeling has proposed it could be tied to fluctuations in intrinsic excitability that could bias the reactivation of previously stored memories [61], or to activity-independent, stochastic synaptic processes [62]. A notable observation is that, coincidentally, drift rates (days and weeks) seem to match the current timescale of BCI decoder calibration[59], although this observation has not been systematically characterized.

Our second proposition is that as subjects learn to reinforce neural activity patterns during early BCI learning, BTSP-mediated changes in neural selectivity to the decoded variable(s) would be characterized by rapid reduction in variability in these activity patterns. During this early phase, neural activity essentially transitions from a highly irregular pattern to a highly regular and repeatable patterns with smaller variability during later intervals. This transition is desirable as it helps BCI source signals reduce variability necessary to stabilize the decoder output. However, it comes at a cost; maintaining these steady activity levels with reduced variability triggers intrinsic plasticity (IP) – an activity-dependent change in single neurons' excitability in response to repeated depolarizing inputs.

IP has been widely documented in neocortex [63], cerebellum [64,65], hippocampus [66], among other areas [67]. Despite being mostly characterized in brain slices *ex vivo* in which real physiologic

signals such as motivation, attention, and reward are absent (but see [68]), it has been postulated as a way for neurons to instantly adapt their spiking output to maintain their membrane voltage within a limited dynamic regime – known as a homeostatic state[69,70]. Neurons do so by changing a key structural parameter: the number of ion channel proteins present at the membrane, which occurs over a slow time scale of hours to days. It is believed that the cascade of these processes enables neurons to maintain stability and robustness of recently learned experiences and become more resilient to noise [71-73]. However, this new network state and the ensuing spontaneous activity – in which cortex revisits specific neural patterns due to oscillations within cortical microcircuits [74] – locally drives further synaptic plasticity[75], and results in a re-organized neural circuit [76].

Our third proposition is that BTSP followed by IP alters the homestatic state of the network in which BCI neurons are embedded and thus necessitates synaptic scaling [46,70,75,77-80]. This is a process in which neurons re-adjust the strength of their synapses through glutamate receptor trafficking outside of behavior to stabilize firing rates [78]. This alteration seems to be cell and synapse type [81], area and region specific [78], depending on the neural circuit connectivity and dynamics [82,83]. The stochastic fluctuations of inputs to these neurons and altered synaptic efficacies outside of BCI training pave the way for representational drift to manifest in the form of altered spiking statistics, eventually requiring frequent decoder calibration [19,84,85].

Methods

We first designed an experiment to test the idea that both BTSP and IP can be triggered in persistently active neurons over behaviorally relevant time scales (seconds to minutes). We performed two photon (2p) Ca^{2+} imaging of layer 2/3 excitatory neurons in head-fixed mice during wakefulness, aroused state. Transgenic reporter mice (Ai162, TIT2L-GC6s-ICL-tTA2-D, JAX labs) were injected with a viral vector (AAV8-CamKIIa-ChRMine-mScarlett-kv2.1) to express the soma targeted light sensitive opsin, $ChRmine_{Kv2.1}$[86], in excitatory cell types expressing the genetically encoded Ca^{2+} indicator, GCaMP7s [87], followed by an implantation of a cranial glass window (4 mm diameter) over the injection site. After allowing 4-6 weeks for expression, animals were head-fixed under the 2p microscope (Bruker Ultima, WI) and the imaged Field of View (FOV, 900 µm x 900 µm) was screened for regions of interest (ROIs) between ~100 and ~250 µm below the cortical surface that co-express GCaMP7s and $ChRmine_{Kv2.1}$. For each $GCaMP7s^+$ and $ChRmine_{Kv2.1}^+$ neuron selected, we determined the lowest laser power (A_{OL}) and optical pulse duration (PW_{OL}) (λ=1040 nm) that depolarizes the soma, measured as a significant change in evoked Ca^{2+} $\Delta f/f$ (λ=920 nm) relative to background activity (Supplementary methods).

To mimic the integrated input needed for maintaining persistent, repeatable spiking activity patterns typically observed in BCI experiments, we designed a protocol for closed loop control of photostimulation based on somatic Ca^{2+} readout to maintain the cell's activity at a specific target level for a predefined interval. Intracellular somatic Ca^{2+} has been shown to be a reliable indicator of a cell's spiking history, including dendritic plateau potentials[88,89]. This approach - referred to herein as an 'optical clamp'[90]- permitted studying both transient and steady state response of individual cells to repeated depolarizing inputs *in vivo*. We then quantified the extent to which non-clamped neurons within the same FOV exhibited significant change in their activity dynamics as a result of clamping one or more neurons.

Figure 2: Experimental protocol to induce BTSP and IP in single neurons *in vivo*

BCI control in vivo

We next designed an experiment in which water restricted mice expressing GCaMP7s in excitatory neurons in layer 2/3 (L2/3) primary visual cortex (V1) were trained to volitionally modulate the activity of multiple ensembles of neurons for water rewards. Given an ensemble, the animal was rewarded for modulating the average firing of a positive target pair (N+) above that of a negative target pair (N-) beyond a set threshold T1. Experiments were carried out over a number of sessions spanning multiple consecutive and non-consecutive days in which we alternated between ensembles that were either disjoint, partially or fully overlapping to quantify learning both within as well as across sessions (Supplementary methods).

Results

We first tested whether single neurons could be optically clamped at different Ca^{2+} target levels for preset time intervals. After optimizing the optical stimulation parameters (pulse amplitude, pulse width and laser power) for each cell, we found that cells could be reliably maintained at target activity levels for many minutes following clamp onset (Figure 3B). We also found that multiple 'target' cells could be 'yoked' together with 'trigger' cells' Ca^{2+} activity (Figure 3D), consistent with published reports [91]. We also verified that off-target stimulation of adjacent cell bodies and/or neuropils was minimal to none (Figures 3E-3F).

Figure 3 Closed loop protocol for all-optical, activity-dependent modulation of neural activity

We then asked whether the single cell optical clamp over behavioral time scales alters somatic Ca^{2+} signals in a way that mirrors the changes in the plateau potentials consistent with the timescale governing BTSP. We reasoned that backpropagating action potentials (bAPs, which are ~1 millisecond in duration[92]) evoked by depolarizing current injection into the soma result in broad subthreshold dendritic signals that are linearly associated with the number of action potentials produced at the soma, consistent with published work[42,93]. These bAPs are known to spread along proximal dendrites with noticeable attenuation at the farthest imaged locations [88]. Furthermore, following long depolarization, the somatic Ca^{2+} peak is expected to attenuate consistent with adaptation mechanisms associated with the reciprocal interaction between local dendritic spikes and depolarization-induced suppression of excitation[88]. Thus, somatic depolarization in response to a single light pulse could be used as a proxy signal to estimate the changes associated with dendritic plateau potential following the optical clamp.

We stimulated each cell 4-5 times using a single pulse (50 ms, 5 spirals) separated by 15 seconds (total duration ~ 1 min) and averaged the evoked Ca^{2+} traces to obtain a baseline for the global plateau potential before the optical clamp. We repeated the same step at 3 min and 8 min after cessation of the clamp. We found that when a cell is optically clamped for ~200 sec (at 5*SD above its average baseline fluorescence), the evoked Ca^{2+} amplitude decreased by ~18% (Figure 4A). Notably the decay time constant τ_e effectively decreased the response to 37% of its peak within 2257 ms ± 132.2 ms of the pre clamp window to 1850 ms ± 150.3 ms post clamp, consistent with BTSP models[41]. This signal on its own does not result in synaptic potentiation[94]. However, the overlap between this global signal and the local input signal at the dendritic compartment

determines the degree of synaptic weight change for that input. Note that because our protocol relied on depolarizing the soma rather than the targeted activation of specific dendritic compartments, we could not measure the rise time of the plateau signal to verify its expected asymmetry [41]. Nonetheless, the decay time produced in our model agrees closely with published studies.

Across multiple experiments, we also found that the decrease in peak Ca^{2+} amplitude α_e at 3*SD target level was significant at 3 min (before vs post-3min: *p=0.011035) but partially rebounded at 8 mins (before vs post-8min:p=0.065906; post-3min vs post-8min: p=0.47326), suggesting the effect is transient (n=3 cells, N=3 mice; Figure 4B). The effect was more pronounced at 5*SD target level (before vs post-3min: ***p= 0.00010167) with slower rebound to pre-clamp levels (before vs post-8min: *p=0.015294; post-3min vs post-8min: p=0.1656) (n=7 cells, N=3 mice; Figure 4D). The changes observed in peak Ca2+ amplitude were mirrored by similar changes in decay time constant τ_e. Specifically, we observed a significant decrease in τ_e at 3 SD target level (before vs post-3min:***p=0.00051785; before vs post-8min: p=0.31263; post-3min vs post-8min: *p=0.0032513) (Figure 4C). At 5*SD target level, τ_e significantly decreased (before vs post-3min:***p=4.9042e-05) and took longer to rebound (before vs post-8min: *p=0.024711; post-3min vs post-8min: p=0.076848; Figure 4E). These results suggest that Ca^{2+} dynamics are a function of the target level during clamp and support the idea that intracellular Ca2+ can serve as readout of the neuron's activity in recent history. Furthermore, the observed effects are in general agreement with published work suggesting that after-hyperpolarizing current is depressed due to reduced postsynaptic CaMKII signaling [95]. However, it is released gradually and reach baseline levels after one hour, a timing that coincides with the enrichment of several postsynaptic proteins to pre-plasticity levels[96]. These results suggest that a synaptic eligibility trace is generated that lasts for seconds to minutes following removal of a repeated depolarizing input.

Figure 4 Characterization of somatic Ca^{2+} response to open loop stimulation

We then asked to what extent the evoked Ca^{2+} response changes once the feedback control loop is closed, i.e., during optical clamp. We performed the optical clamp at multiple target activity levels (A_{CL} = 1, 3 and 5*SD) for a preset interval (T_{CL} = 266 sec). Because the evoked Ca^{+2} response amplitude and decay time is measured during closed loop, characterizing the inter-stimulation interval (ISI) provides insight into how the cell adapts quickly to each new target. We consistently observed that the ISI was highly variable early during the clamp but later stabilized. To quantify these effects, we defined a *transient state* as the time interval from clamp onset during which the ISI variance is greater than 10% of its value at steady state. We expected that the larger the difference between the baseline activity level (before clamp) and the target activity level, the faster the response transition would be from the transient to the steady state dynamics. Simply stated, neurons are expected to adapt more rapidly (shorter decay time) to strong and persistent inputs, i.e. higher target level, compared to weak and sparse inputs. First, we found that the ISI variance was significantly higher in the first 60-sec compared to the subsequent second, third and fourth 60-sec intervals (Figure 5A). This trend was similar across all cells examined (n=5 cells, N=4 mice, Figure 5B). However, no significant differences were found between the second, third or fourth intervals for either the 3*SD or the 5 *SD cases. This trend

persisted across all cells examined (Figure 5C-D). We also found that the ISI variance for 5*SD target level was significantly lower than the 3*SD level (Figure 5E), but there was no significant difference above 180 sec. These results suggest that 1) the transition from early, largely irregular response to late, sustained and more regular response can be used to quantify how rapidly a cell adapts to specific target activity; the higher the target level the faster the adaptation and, 2) the time scale of this adaptation only lasts for 2-3 minutes. These transitions are likely cell dependent due to different morphologies and dendritic structures[88].

Figure 5: Characterization of somatic Ca^{2+} response to closed loop stimulation

We then asked whether the changes observed under both open and closed loop photostimulation are associated with changes in the f-I characteristics. We performed two-photon guided whole cell recording of select neurons and implemented the protocol in Figure 2. We then probed the cell's input/output function by systematically varying the input power and measuring the spike rate (Figure 6A-B). We found that the f-I characteristics shifted significantly to the right following clamp. These results suggest more response suppression took place consistent with prior work. They further suggest sublinearity at higher inputs takes place following periods of persistent activity. We also asked whether a computational model could capture these effects. We found that a Boltzman function model with two parameters[97], the adaptation time constant τ_a and the adaptation strength α can disentangle the relative contributions of each element of the feedback loop that relates the cell's firing rate to the Ca^{2+} influx driven by the input current (Supplementary Figure 1) .

Figure 6: Characterization of changes in intrinsic excitability before and after optical clamp

We then asked whether clamping one cell's activity at a particular target level has any influence on other adjacent cells within the same FOV. Recent studies have suggested that neurons within layer 2/3 of the primary visual cortex (V1) with similar stimulus feature selectivity are more likely to be synaptically connected compared to cells that have dissimilar tuning [98]. We clamped one cell at different target levels and quantified the changes in Ca^{2+} in the other imaged ROIs in terms of peak fluorescence and decay time constant during clamp. We found a significant increase in Ca^{2+} fluorescence intensity and decay time constant in n=17/46 cells response to target level (5*SD) ($p = 0.0011$; two-sided t-test), and for target level (3*SD) n=9/46; $p= 0.0045$; two-sided t-test) (Figure 7, Supplementary figure 2). While our experimental design did not permit mapping synaptic connectivity between the imaged neurons, published reports [98] suggests that optically triggering action potentials in a targeted neuron and directly measuring its functional influence on neighboring, non-targeted neurons can be used to assess synaptic connectivity profiles and accordingly make predictions about the extent of synaptic scaling taking place over longer periods.

Figure 7 Influence of clamped neuron on adjacent neurons within the same FOV

Finally, we asked whether the above findings carry over to actual behavioral experiments of BCI learning and skill consolidation. We trained mice on a 1-dimensional BCI cursor control over many weeks (supplementary methods). In six separate non-consecutive sessions, we selected six different ensembles of four neurons each (Figure 8A), and used a decoder filter to calculate the position of the neural cursor at each time step. Following an initial random cursor location at the start of each trial, the animal was rewarded if neuron pair N+=(N1& N2) increases the firing rates while neuron pair N-=(N3, N4) decreases the firing rates until the cursor attains the target. Thus, the animal had different strategies to attain a target; for example, it could activate either or both neurons of the group N+ or decrease the activity of neurons in the group N-. Moreover, even if N+ neurons increase their activity, the activity of neurons in N- may be elevated enough to prevent the neural cursor from reaching the target. As a result, not all ensemble neurons were active at the time of target acquisition and not all activation of ensemble neurons resulted in a target.

We first examined the animal's behavior within the first training session for each ensemble (Figures 8 F&H). Owing to the causal mapping between the BCI neurons and cursor movement, we used a simple behavioral criterion to compare the success rate in the first session for each ensemble to measure the extent to which rapid learning occurs within that ensemble. Our model predicts that re-occurrence of specific spiking patterns would be facilitated by BTSP taking place within a few trials. We set a criterion of 60% success rate to separate weak/slow from strong/rapid learner ensembles. Among the six ensembles investigated (n=24 BCI cells), we found that three ensembles were categorized as weak/slow learners in which within session success rate was ~49% (Figure 8B), with significantly long Time to Target (TT) (n=12, p=0.002). In contrast, the other three ensembles had a success rate of ~92%, with significantly smaller TT (Fig. 8C) (n=12, p=0.0001). These results suggest that leanring might not progress at the same rate in every ensemble, and that the role that each neuron plays within an ensemble may differ across ensembles.

Figure 8 Instantaneous BCI-mediated plasticity within first training session

Our model predicts that with repeated activation of an ensemble, changes in homestatic state can be measured as changes in baseline firing rates across sessions. We selected one of the strong/rapid learner ensembles (ensemble 4) and continued to train the animal on the BCI task for an additional 13 sessions spanning a two-week period. We then compared the firing rate of BCI neurons during behavioral trials. We found no significant change in the N+ group (n=12; two sample t-test; N1: p=0.18, N2: p=0.07) between the first session and the last session (Figure 9A, Supp Fig 3A). These results suggest that the animal did not change its strategy with respect to modulation of the N+ group. In contrast, there was a significant change in the N- group (N3: ***p= 5.6e-10, N4: ***p=2.05e-05). Notably, these changes were opposite to one another; BCI neuron N3 decreased its firing whereas BCI neuron N4 increased its firing such that the net result among the N- pair was negligible, resulting in similar performance (90% in session 1 and 98% in the last session). We also found no significant changes in non-BCI neurons's spiking probability during behavior (Supplementary Figures 3). These results suggest that the animal changed its

strategy for modulating the N- pair between the two sessions that were examined albeit this change had no net effect on behavior.

To further examine changes in homeostatic states, we compared spiking probabilities and firing rate (outside the task) of neurons within the same ensemble around the early and late sessions (supplementary methods). We found significant changes in BCI neurons 1-3 (***p=8.6e-10, ***p=7.72e-13, ****p= 5.75e-15) but not for N4 (p=0.68) (Fig 9B). We also found similar trends in non-BCI neurons within the same FOV (Fig 9C, supplementary Figure 4). These results suggest that some BCI neurons recruited during learning undergo changes in homeostatic firing, depending on the strategy used by the animal to optimize control. These changes could also affect non-BCI neurons within the local circuit as our analysis of non-clamped neurons within the same local area has shown (Figure 7; supplementary figure 2).

Figure 9 Longitudinal assessment of changes across BCI training sessions

Discussion

In this study, we proposed a mechanistic model for BCI learning that might explain multiple observations widely documented but have not received sufficient attention in the BCI community. This metaplasticity model, comprising synergistic interaction between established forms of neuroplasticity, could account for rapid within session learning, representational drift over days and weeks, and BCI skill consolidation demonstrated as preserved performance over multiple sessions despite significant changes in activity dynamics. We developed a novel protocol to probe BTSP and IP that relies on targeted closed loop optical control of single cell activity dynamics and showed that, on the time scale of seconds to minutes, substantial BTSP could be induced. The ensuing changes in neuronal firing statistics are consistent with known reciprocal interaction between local dendritic spikes and depolarization-induced suppression of excitation.

We then showed that following artificial induction of the same activity pattern in single cells using targeted closed loop photostimulation, significant adaptation occurs over 2-3 minutes in response to repeated depolarizing inputs. While this was not surprising given prior reports, we found that this adaptation is a function of the target activity level. These results suggest that maintaining these activity levels rapidly sculpts neurons' dynamics to produce a delimited alteration of firing consistent with the input pattern. This feature could endow single neurons with the capacity for rapid memory formation representing that input pattern. We then showed that over the time scale of minutes following cessation of the clamp, rebounding of Ca^{2+} decay takes place. These results are consistent with the behavior of hyperpolarizing currents that are released gradually and reach baseline levels around the timing of enrichment of several postsynaptic proteins to pre-plasticity levels.

For neurons to engage BTSP, they need to act as a feedback control module that continuously monitors their own firing output in response to a particular input pattern and generates a spatially distributed synaptic eligibility trace consistent with that input via a Ca^{2+} mediated plateau potential. The neuron would then potentiate the inputs corresponding to that trace when they contribute to rewarded actions over seconds long interval[70]. This time window is critical as it permits the 'time to reward' to be simultaneously encoded alongside the eligibility

trace that might last for a few trials [99]. Indeed, prior work using Ca^{2+} imaging in cortical association areas has shown that neurons continue to encode past trial experience[100,101], including reward omissions, suggesting that these eligibility traces are critical for action-outcome history. If the neuron output is within the 'target' level, this global instruction signal should decay relatively fast, as there is no more 'errors' to correct. If the neuron is significantly deviating away from that target level, the instruction signal should last longer to potentiate possible inputs needed to correct these errors.

To decouple the role of reward and potential dopaminergic influence on the induced plasticity, we designed an experiment to characterize this mechanism by mimicking the recurring activity pattern associated with rewarded BCI neurons'– an elevated excitability state – in a closed loop control setting. To simplify the analysis and to avoid potential confounding factors, we simplified these activity patterns to an average target activity level that the neurons needed to maintain above their baseline for a predefined time interval. It is important to note that our goal was not to mimic the full repertoire of activity patterns typically observed during volitional modulation of BCI neurons, but rather to study how different target activity levels that neurons must maintain could result in significant changes in somatic Ca^{2+} that is key to BTSP. We believe this design provided insights into how these signals could be critical in representing the instructive signals in very few trials in a BCI context.

We then provided preliminary evidence supporting the idea that the altered spiking probabilities could trigger changes in the excitability state of the neurons. We have shown that re-occurrence of activity patterns close to the selected target induces IP that shifts the f-I characteristics towards response attenuation and possibly sublinearities. This drift, if persistent, becomes an impediment to BCI control performance because it requires frequent decoder calibration[102].Our modeling results further recapitulated this effect, lending credence to our model structure. We then showed that neurons within the 'broader circuit' may also be influenced by the transient and sustained changes in the homeostatic state of the targeted neurons, despite not being directly targeted by photostimulation. While it was not feasible to map synaptic connectivity between neurons within the local population, we showed that a substantial fraction of the population within the local area can exhibit significant changes in their activity dynamics. Modern approaches, including our own work , to use two photon optogenetics to map synaptic connectivity could play a crucial role in this regard.

Several reports have used recurrent neural network (RNN) models equipped with a reward modulated Hebbian plasticity mechanism to demonstrate that neuromodulators such as dopamine could elongate the time window of integration between efferent and afferent BCI signals to enable learning simple BCI tasks [103-105]. However, with the exception of a recent study [106], these models lack experimental validation and have focused on learning over short timescales (i.e. within minutes to hours[15,82]). It is also inconceivable that determining which synapses to update (the credit assignment problem[107,108]) within the deluge of synaptic connections to BCI neurons can take place within a few minutes. As such, BTSP offers a more plausible mechanism that uses sensory feedback from the cursor's current state to tag the synapses to BCI neurons that caused that state earlier in time, thereby permitting temporally specific information to act on local synapses deemed critical to potentiate (or depress)[109].

We further provided support for our model by investigating both short and long term changes in firing characteristics in an actual behavioral experiment. We first demonstrated that

animals might not be able to learn rapidly with *any* ensemble. We then showed that the animal's performance within the first few trials is a good predictor of their performance later in the trial and in subsequent sessions. These observations were supported by the ability of the animal to adopt a strategy based on how single neurons' excitability could be rapidly altered. To preserve the E/I balance, synaptic scaling must slowly take place at the network level, which likely involves non-BCI neurons to forge new 'attractor' states that can be rapidly attained with repeated practice.

Our study nevertheless has important limitations. First, we used photostimulation to maintain single neurons at activity levels *above* their baseline level. A topic for future work would be to design the experiment to also photoinhibit neurons *below* their baseline level that would mimic participation in decoding rules requiring differential modulation[110-112], rather than integration, of individual neurons' activities, such as the rule we used here. Second, we characterized BTSP and IP in a small sample of the excitatory neurons class in V1 and PPC [5,113]. We only tested the extent to which the clamp protocol causes neuronal adaptation to repeated inputs through habituation (response attenuation) but not sensitization (response enhancement). It would be important to extend the current work to larger sample size and other neuronal cell types, e.g. inhibitory cells, that are known to be sensitized to repeated inputs[70], as well as in other brain areas known to be primary sources of BCI signals (e.g. motor cortex).

While the specific trends observed in implantable BCI experiments have been documented using mostly motoric, the mechanisms discussed extend beyond motor systems, for e.g., hippocampus, [41]. We therefore believe that our work is the first to propose a link between rapid learning, representational drift, and BCI skill consolidation using a metaplasticity model that includes behavioral time scale synaptic plasticity, intrinsic plasticity and synaptic scaling. Because of the causal nature of the transformation from neuronal activity to control signals that is unique to BCIs, BCI experiments have shed a lot more insights into how these disparate mechanisms could be working in synergy to facilitate learning and skill consolidation.

In summary, our findings are critical to understand current limitations of BCI technology that impedes its progress and deployment in clinical and consumer applications. We propose that it an important step towards full autonomy of BCIs in everyday use would be to use neuroplasticity models like the one we propose here, combined with models of anticipated BCI use by the subject, to develop large scale, AI-powered brain-behavior BCI models that inform how decoders should *self-adapt* outside of actual BCI use. They would then be deployed regularly for use by the subject who might arguably find it less cognitively demanding to control and streamline its use in daily living.

Acknowledgment

This study was supported by NINDS grant # NS93909. We thank the anonymous reviewers for their helpful comments.

The research has been conducted following NIH guidelines for research involving vertebrate animals under University of Florida's approved IACUC Protocol # 202009788

References

1 Hochberg, L. R. *et al.* Neuronal ensemble control of prosthetic devices by a human with tetraplegia. *Nature* **442**, 164-171 (2006).

2 Collinger, J. L. *et al.* High-performance neuroprosthetic control by an individual with tetraplegia. *Lancet* **381**, 557-564, doi:10.1016/S0140-6736(12)61816-9 (2013).

3 Wodlinger, B. *et al.* Ten-dimensional anthropomorphic arm control in a human brain-machine interface: difficulties, solutions, and limitations. *J Neural Eng* **12**, 016011, doi:10.1088/1741-2560/12/1/016011 (2015).

4 Collinger, J. L. *et al.* Collaborative approach in the development of high-performance brain-computer interfaces for a neuroprosthetic arm: translation from animal models to human control. *Clinical and translational science* **7**, 52-59, doi:10.1111/cts.12086 (2014).

5 Guan, C. *et al.* Decoding and geometry of ten finger movements in human posterior parietal cortex and motor cortex. *J Neural Eng* **20**, doi:10.1088/1741-2552/acd3b1 (2023).

6 Saha, S. *et al.* Progress in brain computer interface: Challenges and opportunities. *Frontiers in systems neuroscience* **15**, 578875 (2021).

7 Oweiss, K. G. & Badreldin, I. S. Neuroplasticity subserving the operation of brain-machine interfaces. *Neurobiol Dis* **83**, 161-171, doi:10.1016/j.nbd.2015.05.001 (2015).

8 Shenoy, K. V. & Carmena, J. M. Combining decoder design and neural adaptation in brain-machine interfaces. *Neuron* **84**, 665-680, doi:10.1016/j.neuron.2014.08.038 (2014).

9 Wander, J. D. *et al.* Distributed cortical adaptation during learning of a brain–computer interface task. *Proceedings of the National Academy of Sciences* **110**, 10818-10823 (2013).

10 Gilja, V. *et al.* A high-performance neural prosthesis enabled by control algorithm design. *Nat Neurosci* **15**, 1752-1757, doi:10.1038/nn.3265 (2012).

11 Vaidya, M. *et al.* Emergent coordination underlying learning to reach to grasp with a brain-machine interface. *J Neurophysiol* **119**, 1291-1304, doi:10.1152/jn.00982.2016 (2018).

12 Balasubramanian, K. *et al.* Changes in cortical network connectivity with long-term brain-machine interface exposure after chronic amputation. *Nat Commun* **8**, 1796, doi:10.1038/s41467-017-01909-2 (2017).

13 Oweiss, K. G. & Badreldin, I. S. Neuroplasticity subserving the operation of brain–machine interfaces. *Neurobiology of disease* **83**, 161-171 (2015).

14 Perich, M. G., Gallego, J. A. & Miller, L. E. A Neural Population Mechanism for Rapid Learning. *Neuron* **100**, 964-976 e967, doi:10.1016/j.neuron.2018.09.030 (2018).

15 Sadtler, P. T. *et al.* Neural constraints on learning. *Nature* **512**, 423-426, doi:10.1038/nature13665 (2014).

16 Oby, E. R. *et al.* New neural activity patterns emerge with long-term learning. *Proc Natl Acad Sci U S A* **116**, 15210-15215, doi:10.1073/pnas.1820296116 (2019).

17 Grosse-Wentrup, M., Mattia, D. & Oweiss, K. Using brain-computer interfaces to induce neural plasticity and restore function. *J Neural Eng* **8**, 025004, doi:10.1088/1741-2560/8/2/025004 (2011).

18 Badreldin, I. *et al.* in *IEEE Int. Conference on Neural Engineering* Vol. in press (IEEE, San Diego, CA, 2013).

19 Orsborn, Amy L. *et al.* Closed-Loop Decoder Adaptation Shapes Neural Plasticity for Skillful Neuroprosthetic Control. *Neuron* **82**, 1380-1393, doi:10.1016/j.neuron.2014.04.048 (2014).

20 Jackson, A., Mavoori, J. & Fetz, E. Motor cortex plasticity induced by an implanted neural prosthesis. *Neurosci Res* **55**, S15-S15 (2006).

21 Jackson, A., Mavoori, J. & Fetz, E. E. Long-term motor cortex plasticity induced by an electronic neural implant. *Nature* **444**, 56-60, doi:10.1038/nature05226 (2006).

22 Caporale, N. & Dan, Y. Spike Timing Dependent Plasticity: A Hebbian Learning Rule. *Annual Review of Neuroscience* **31**, 25-46 (2008).

23 Dan, Y. & Poo, M. M. Spike Timing-Dependent Plasticity: From Synapse to Perception. *Physiological Reviews* **86**, 1033 (2006).

24 Abbott, L. F. & Nelson, S. B. Synaptic plasticity: taming the beast. *Nature Neuroscience* **3**, 1178-1183, doi:10.1038/81453 (2000).

25 Rebesco, J. M., Stevenson, I. H., Kording, K. P., Solla, S. A. & Miller, L. E. Rewiring neural interactions by micro-stimulation. *Frontiers in systems neuroscience* **4**, doi:10.3389/fnsys.2010.00039 (2010).

26 Brzosko, Z., Mierau, S. B. & Paulsen, O. Neuromodulation of Spike-Timing-Dependent plasticity: past, present, and future. *Neuron* **103**, 563-581 (2019).

27 Bensmaia, S. J. & Miller, L. E. Restoring sensorimotor function through intracortical interfaces: progress and looming challenges. *Nat Rev Neurosci* **15**, 313-325, doi:10.1038/nrn3724 (2014).

28 Kempter, R., Gerstner, W. & Van Hemmen, J. L. Hebbian learning and spiking neurons. *Phys Rev E* **59**, 4498 (1999).

29 Song, S., Miller, K. D. & Abbott, L. F. Competitive Hebbian learning through spike-timing-dependent synaptic plasticity. *Nature neuroscience* **3**, 919-926 (2000).

30 Qin, S. *et al.* Coordinated drift of receptive fields in Hebbian/anti-Hebbian network models during noisy representation learning. *Nature Neuroscience* **26**, 339-349 (2023).

31 Driscoll, L. N., Duncker, L. & Harvey, C. D. Representational drift: Emerging theories for continual learning and experimental future directions. *Curr Opin Neurobiol* **76**, 102609, doi:10.1016/j.conb.2022.102609 (2022).

32 Driscoll, L. N., Pettit, N. L., Minderer, M., Chettih, S. N. & Harvey, C. D. Dynamic reorganization of neuronal activity patterns in parietal cortex. *Cell* **170**, 986-999. e916 (2017).

33 Marks, T. D. & Goard, M. J. Stimulus-dependent representational drift in primary visual cortex. *Nature communications* **12**, 5169 (2021).

34 Schoonover, C. E., Ohashi, S. N., Axel, R. & Fink, A. J. Representational drift in primary olfactory cortex. *Nature* **594**, 541-546 (2021).

35 Ziv, Y. *et al.* Long-term dynamics of CA1 hippocampal place codes. *Nature neuroscience* **16**, 264-266 (2013).

36 Driscoll, L. N., Pettit, N. L., Minderer, M., Chettih, S. N. & Harvey, C. D. Dynamic Reorganization of Neuronal Activity Patterns in Parietal Cortex. *Cell* **170**, 986-999 e916, doi:10.1016/j.cell.2017.07.021 (2017).

37 Willsey, M. S. *et al.* Real-time brain-machine interface in non-human primates achieves high-velocity prosthetic finger movements using a shallow feedforward neural network decoder. *Nature Communications* **13**, 6899 (2022).

38 Hayashi, I., Irie, H. & Tsuruse, S. Bagging Algorithm Based on Possibilistic Data Interpolation for Brain-Computer Interface. *Journal of Advanced Computational Intelligence and Intelligent Informatics* **28**, 623-633 (2024).

39 Pun, T. K. *et al.* Measuring instability in chronic human intracortical neural recordings towards stable, long-term brain-computer interfaces. *Communications Biology* **7**, 1363 (2024).

40 Gilja, V. *et al.* Clinical translation of a high-performance neural prosthesis. *Nature medicine* (2015).

41 Bittner, K. C., Milstein, A. D., Grienberger, C., Romani, S. & Magee, J. C. Behavioral time scale synaptic plasticity underlies CA1 place fields. *Science* **357**, 1033-1036, doi:10.1126/science.aan3846 (2017).

42 Markram, H., Lubke, J., Frotscher, M. & Sakmann, B. Regulation of synaptic efficacy by coincidence of postsynaptic APs and EPSPs. *Science* **275**, 213-215 (1997).

43 Li, G., McLaughlin, D. W. & Peskin, C. S. A biochemical description of postsynaptic plasticity—with timescales ranging from milliseconds to seconds. *Proceedings of the National Academy of Sciences* **121**, e2311709121 (2024).

44 Jain, A. *et al.* Dendritic, delayed, stochastic CaMKII activation in behavioural time scale plasticity. *Nature*, 1-9 (2024).

45 Yagishita, S. *et al.* A critical time window for dopamine actions on the structural plasticity of dendritic spines. *Science* **345**, 1616-1620 (2014).

46 Turrigiano, G. G. & Nelson, S. B. Homeostatic plasticity in the developing nervous system. *Nature Reviews Neuroscience* **5**, 97-107 (2004).

47 Keck, T. *et al.* Synaptic scaling and homeostatic plasticity in the mouse visual cortex in vivo. *Neuron* **80**, 327-334, doi:10.1016/j.neuron.2013.08.018 (2013).

48 Milstein, A. D. *et al.* Bidirectional synaptic plasticity rapidly modifies hippocampal representations. *Elife* **10**, e73046 (2021).

49 Fan, L. Z. *et al.* All-optical physiology resolves a synaptic basis for behavioral timescale plasticity. *Cell* **186**, 543-559 e519, doi:10.1016/j.cell.2022.12.035 (2023).

50 Fetz, E. B. & Finocchi.Dv. Operant Conditioning of Specific Patterns of Neural and Muscular Activity. *Science* **174**, 431-& (1971).

51 Kaufman, M. T., Churchland, M. M., Ryu, S. I. & Shenoy, K. V. Cortical activity in the null space: permitting preparation without movement. *Nature neuroscience* **17**, 440-448 (2014).

52 Daly, J., Liu, J., Aghagolzadeh, M. & Oweiss, K. Optimal space–time precoding of artificial sensory feedback through mutichannel microstimulation in bi-directional brain–machine interfaces. *Journal of neural engineering* **9**, 065004 (2012).

53 Sombeck, J. T. *et al.* Characterizing the short-latency evoked response to intracortical microstimulation across a multi-electrode array. *Journal of Neural Engineering* **19**, 026044 (2022).

54 Schultz, W., Dayan, P. & Montague, P. R. A neural substrate of prediction and reward. *Science* **275**, 1593-1599, doi:10.1126/science.275.5306.1593 (1997).

55 Morita, K., Morishima, M., Sakai, K. & Kawaguchi, Y. Reinforcement Learning: Computing the Temporal Difference of Values via Distinct Corticostriatal Pathways: (Trends in Neurosciences 35, 457-467; 2012). *Trends Neurosci* **40**, 453, doi:10.1016/j.tins.2017.05.006 (2017).

56 Pun, T. K. *et al.* Measuring instability in chronic human intracortical neural recordings towards stable, long-term brain-computer interfaces. *Commun Biol* **7**, 1363, doi:10.1038/s42003-024-06784-4 (2024).

57 Oweiss, K., Wise, M., Lopez, C., Wiler, J. & Anderson, D. in *Proceedings of the First Joint BMES/EMBS Conference. 1999 IEEE Engineering in Medicine and Biology 21st Annual Conference and the 1999 Annual Fall Meeting of the Biomedical Engineering Society (Cat. N.* 453 vol. 451 (IEEE).

58 Polikov, V. S., Tresco, P. A. & Reichert, W. M. Response of brain tissue to chronically implanted neural electrodes. *J Neurosci Methods* **148**, 1-18, doi:10.1016/j.jneumeth.2005.08.015 (2005).

59 Eleryan, A. *et al.* Tracking single units in chronic, large scale, neural recordings for brain machine interface applications. *Front Neuroeng* **7**, 23, doi:10.3389/fneng.2014.00023 (2014).

60 Rule, M. E. *et al.* Stable task information from an unstable neural population. *elife* **9**, e51121 (2020).

61 Lois, C., Wang, B., Torok, Z. & Fairhall, A. Unsupervised Restoration of a Complex Learned Behavior After Large-Scale Neuronal Perturbation. (2022).

62 Eppler, J.-B., Lai, T., Aschauer, D., Rumpel, S. & Kaschube, M. Representational drift reflects ongoing balancing of stochastic changes by Hebbian learning. *bioRxiv*, 2025.2001.2005.631363, doi:10.1101/2025.01.05.631363 (2025).

63 Desai, N. S., Rutherford, L. C. & Turrigiano, G. G. Plasticity in the intrinsic excitability of cortical pyramidal neurons. *Nat Neurosci* **2**, 515-520, doi:10.1038/9165 (1999).

64 Shim, H. G., Lee, Y.-S. & Kim, S. J. The emerging concept of intrinsic plasticity: activity-dependent modulation of intrinsic excitability in cerebellar Purkinje cells and motor learning. *Experimental neurobiology* **27**, 139 (2018).

65 Brickley, S. G., Revilla, V., Cull-Candy, S. G., Wisden, W. & Farrant, M. Adaptive regulation of neuronal excitability by a voltage-independent potassium conductance. *Nature* **409**, 88-92, doi:10.1038/35051086 (2001).

66 Fan, Y. *et al.* Activity-dependent decrease of excitability in rat hippocampal neurons through increases in I h. *Nature neuroscience* **8**, 1542-1551 (2005).

67 Debanne, D., Inglebert, Y. & Russier, M. Plasticity of intrinsic neuronal excitability. *Current opinion in neurobiology* **54**, 73-82 (2019).

68 Kerr, J. N., Greenberg, D. & Helmchen, F. Imaging input and output of neocortical networks in vivo. *Proc Natl Acad Sci U S A* **102**, 14063-14068, doi:0506029102 [pii] 10.1073/pnas.0506029102 (2005).

69 Marder, E. & Goaillard, J.-M. Variability, compensation and homeostasis in neuron and network function. *Nature Reviews Neuroscience* **7**, 563-574, doi:10.1038/nrn1949 (2006).

70 Marom, S. & Marder, E. A biophysical perspective on the resilience of neuronal excitability across timescales. *Nat Rev Neurosci* **24**, 640-652, doi:10.1038/s41583-023-00730-9 (2023).

71 Gainey, M. A. & Feldman, D. E. Multiple shared mechanisms for homeostatic plasticity in rodent somatosensory and visual cortex. *Philosophical Transactions of the Royal Society B: Biological Sciences* **372**, 20160157 (2017).

72 Turrigiano, G. Homeostatic synaptic plasticity: local and global mechanisms for stabilizing neuronal function. *Cold Spring Harbor perspectives in biology* **4**, a005736 (2012).

73 Wefelmeyer, W., Puhl, C. J. & Burrone, J. Homeostatic plasticity of subcellular neuronal structures: from inputs to outputs. *Trends in neurosciences* **39**, 656-667 (2016).

74 Fries, P., Neuenschwander, S., Engel, A. K., Goebel, R. & Singer, W. Rapid feature selective neuronal synchronization through correlated latency shifting. *Nature neuroscience* **4**, 194-200 (2001).

75 Winnubst, J., Cheyne, J. E., Niculescu, D. & Lohmann, C. Spontaneous activity drives local synaptic plasticity in vivo. *Neuron* **87**, 399-410 (2015).

76 Inagaki, H. K., Fontolan, L., Romani, S. & Svoboda, K. Discrete attractor dynamics underlies persistent activity in the frontal cortex. *Nature* **566**, 212-217, doi:10.1038/s41586-019-0919-7 (2019).

77 Hengen, K. B., Lambo, M. E., Van Hooser, S. D., Katz, D. B. & Turrigiano, G. G. Firing rate homeostasis in visual cortex of freely behaving rodents. *Neuron* **80**, 335-342, doi:10.1016/j.neuron.2013.08.038 (2013).

78 Turrigiano, G. G. The self-tuning neuron: synaptic scaling of excitatory synapses. *Cell* **135**, 422-435 (2008).

79 Nelson, S. B., Sjöström, P. J. & Turrigiano, G. G. Rate and timing in cortical synaptic plasticity. *Philos Trans R Soc Lond B Biol Sci.* **357**, 1851-1857 (2002).

80 Turrigiano, G. G. & Nelson, S. B. Hebb and homeostasis in neuronal plasticity. *Current opinion in neurobiology* **10**, 358-364 (2000).

81 Mitani, A., Dong, M. & Komiyama, T. Brain-Computer Interface with Inhibitory Neurons Reveals Subtype-Specific Strategies. *Curr Biol* **28**, 77-83 e74, doi:10.1016/j.cub.2017.11.035 (2018).

82 Golub, M. D. *et al.* Learning by neural reassociation. *Nature neuroscience* **21**, 607-616 (2018).

83 Makino, H., Hwang, E. J., Hedrick, N. G. & Komiyama, T. Circuit Mechanisms of Sensorimotor Learning. *Neuron* **92**, 705-721, doi:10.1016/j.neuron.2016.10.029 (2016).

84 Pandarinath, C. *et al.* High performance communication by people with paralysis using an intracortical brain-computer interface. *Elife* **6**, doi:10.7554/eLife.18554 (2017).

85 Brandman, D. M. *et al.* Rapid calibration of an intracortical brain-computer interface for people with tetraplegia. *J Neural Eng* **15**, 026007, doi:10.1088/1741-2552/aa9ee7 (2018).

86 Marshel, J. H. *et al.* Cortical layer-specific critical dynamics triggering perception. *Science* **365**, doi:10.1126/science.aaw5202 (2019).

87 Shen, Y. *et al.* A genetically encoded Ca(2+) indicator based on circularly permutated sea anemone red fluorescent protein eqFP578. *BMC Biol* **16**, 9, doi:10.1186/s12915-018-0480-0 (2018).
88 Sjostrom, P. J., Rancz, E. A., Roth, A. & Hausser, M. Dendritic excitability and synaptic plasticity. *Physiol Rev* **88**, 769-840, doi:10.1152/physrev.00016.2007 (2008).
89 Sjöström, P. J., Turrigiano, G. G. & Nelson, S. B. Rate, timing, and cooperativity jointly determine cortical synaptic plasticity. *Neuron* **32**, 1149-1164 (2001).
90 Packer, A. M., Russell, L. E., Dalgleish, H. W. & Hausser, M. Simultaneous all-optical manipulation and recording of neural circuit activity with cellular resolution in vivo. *Nat Methods* **12**, 140-146, doi:10.1038/nmeth.3217 (2015).
91 Russell, L. E. *et al.* All-optical interrogation of neural circuits in behaving mice. *Nat Protoc* **17**, 1579-1620, doi:10.1038/s41596-022-00691-w (2022).
92 Hoffman, D. A., Magee, J. C., Colbert, C. M. & Johnston, D. K+ channel regulation of signal propagation in dendrites of hippocampal pyramidal neurons. *Nature* **387**, 869-875 (1997).
93 Markram, H., Helm, P. J. & Sakmann, B. Dendritic calcium transients evoked by single back-propagating action potentials in rat neocortical pyramidal neurons. *J Physiol* **485 (Pt 1)**, 1-20 (1995).
94 Sutton, R. S. & Barto, A. G. Toward a modern theory of adaptive networks: expectation and prediction. *Psychological review* **88**, 135 (1981).
95 Daoudal, G. & Debanne, D. Long-term plasticity of intrinsic excitability: learning rules and mechanisms. *Learning & memory* **10**, 456-465 (2003).
96 Flores, J. C. & Zito, K. A synapse-specific refractory period for plasticity at individual dendritic spines. *bioRxiv*, 2024.2005. 2024.595787 (2024).
97 Benda, J. Neural adaptation. *Current Biology* **31**, R110-R116 (2021).
98 Chettih, S. N. & Harvey, C. D. Single-neuron perturbations reveal feature-specific competition in V1. *Nature* **567**, 334-340, doi:10.1038/s41586-019-0997-6 (2019).
99 Yagishita, S. *et al.* A critical time window for dopamine actions on the structural plasticity of dendritic spines. *Science* **345**, 1616-1620, doi:10.1126/science.1255514 (2014).
100 Hwang, E. J., Dahlen, J. E., Mukundan, M. & Komiyama, T. History-based action selection bias in posterior parietal cortex. *Nature communications* **8**, 1242 (2017).
101 Akrami, A., Kopec, C. D., Diamond, M. E. & Brody, C. D. Posterior parietal cortex represents sensory history and mediates its effects on behaviour. *Nature* **554**, 368-372 (2018).
102 Carmena, J. M. *et al.* Learning to control a brain-machine interface for reaching and grasping by primates. *PLoS Biol* **1**, E42, doi:10.1371/journal.pbio.0000042 (2003).
103 Legenstein, R., Chase, S. M., Schwartz, A. B. & Maass, W. A Reward-Modulated Hebbian Learning Rule Can Explain Experimentally Observed Network Reorganization in a Brain Control Task. *Journal of Neuroscience* **30**, 8400-8410, doi:Doi 10.1523/Jneurosci.4284-09.2010 (2010).
104 Aghagolzadeh, M., Eldawlatly, S. & Oweiss, K. Synergistic Coding by Cortical Neural Ensembles. *Ieee T Inform Theory* **56**, 875-889 (2010).

105 Feulner, B. & Clopath, C. Neural manifold under plasticity in a goal driven learning behaviour. *PLoS Comput Biol* **17**, e1008621, doi:10.1371/journal.pcbi.1008621 (2021).
106 Vendrell-Llopis, N. *et al.* Dopamine D1 receptor activation in the striatum is sufficient to drive reinforcement of anteceding cortical patterns. *Neuron* (2025).
107 Dam, G., Kording, K. & Wei, K. Credit assignment during movement reinforcement learning. *PLoS One* **8**, e55352, doi:10.1371/journal.pone.0055352 (2013).
108 Hamid, A. A., Frank, M. J. & Moore, C. I. Wave-like dopamine dynamics as a mechanism for spatiotemporal credit assignment. *Cell* **184**, 2733-2749 e2716, doi:10.1016/j.cell.2021.03.046 (2021).
109 Li, P. Y. & Roxin, A. Rapid memory encoding in a recurrent network model with behavioral time scale synaptic plasticity. *PLoS Comput Biol* **19**, e1011139, doi:10.1371/journal.pcbi.1011139 (2023).
110 Fetz, E. E. Operant conditioning of cortical unit activity. *Science* **163**, 955-958 (1969).
111 Fetz, E. E. & Baker, M. A. Operantly conditioned patterns on precentral unit activity and correlated responses in adjacent cells and contralateral muscles. *J Neurophysiol* **36**, 179-204 (1973).
112 Athalye, V. R., Santos, F. J., Carmena, J. M. & Costa, R. M. Evidence for a neural law of effect. *Science* **359**, 1024-1029, doi:10.1126/science.aao6058 (2018).
113 Andersen, R. A., Musallam, S. & Pesaran, B. Selecting the signals for a brain-machine interface. *Curr Opin Neurobiol* **14**, 720-726, doi:10.1016/j.conb.2004.10.005 (2004).

Figures

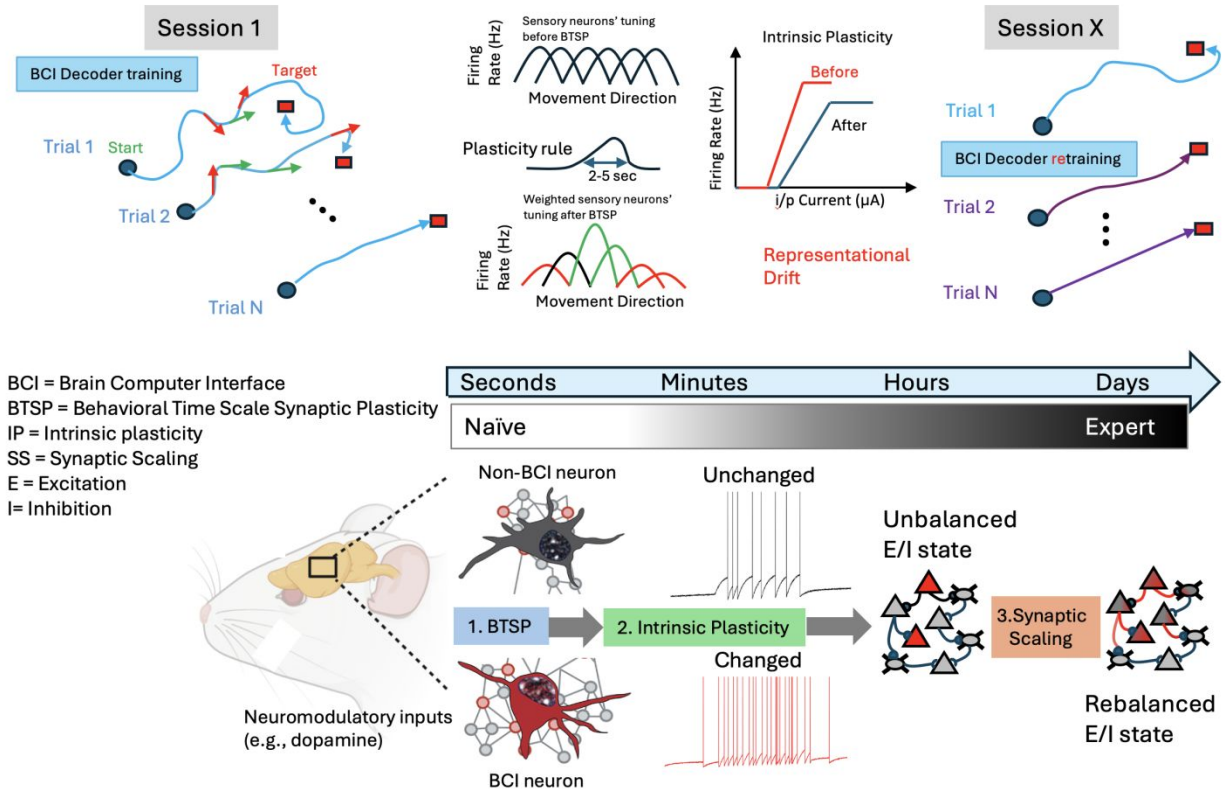

Figure 1

Metaplasticity model for BCI learning and skill consolidation featuring interaction between three elements: behavioral time scale synaptic plasticity (BTSP), intrinsic plasticity (IP) and synaptic scaling (SS) taking place over a multitude of time scales. During the first training session, rewarded neural activity patterns result in an increase in their frequency over seconds to minutes. Through neuromodulatory influence and repeated activation, changes in intrinsic excitability result and may persist over longer periods of hours, depending on the frequency of training. The shift from this homeostatic state leads to an unbalanced excitation/inhibition (E/I) state within local circuits that could affect non-BCI neurons. The balance is eventually restored through synaptic scaling over much slower time scales of days and weeks. The restoration of this balance might not re-instate the original excitability state of each individual cell but may result in a new 'attractor' state of the ensemble. These changes could explain the representational drift typically observed over similar time scales that adversely affects BCI performance and requires repeated BCI decoder calibration.

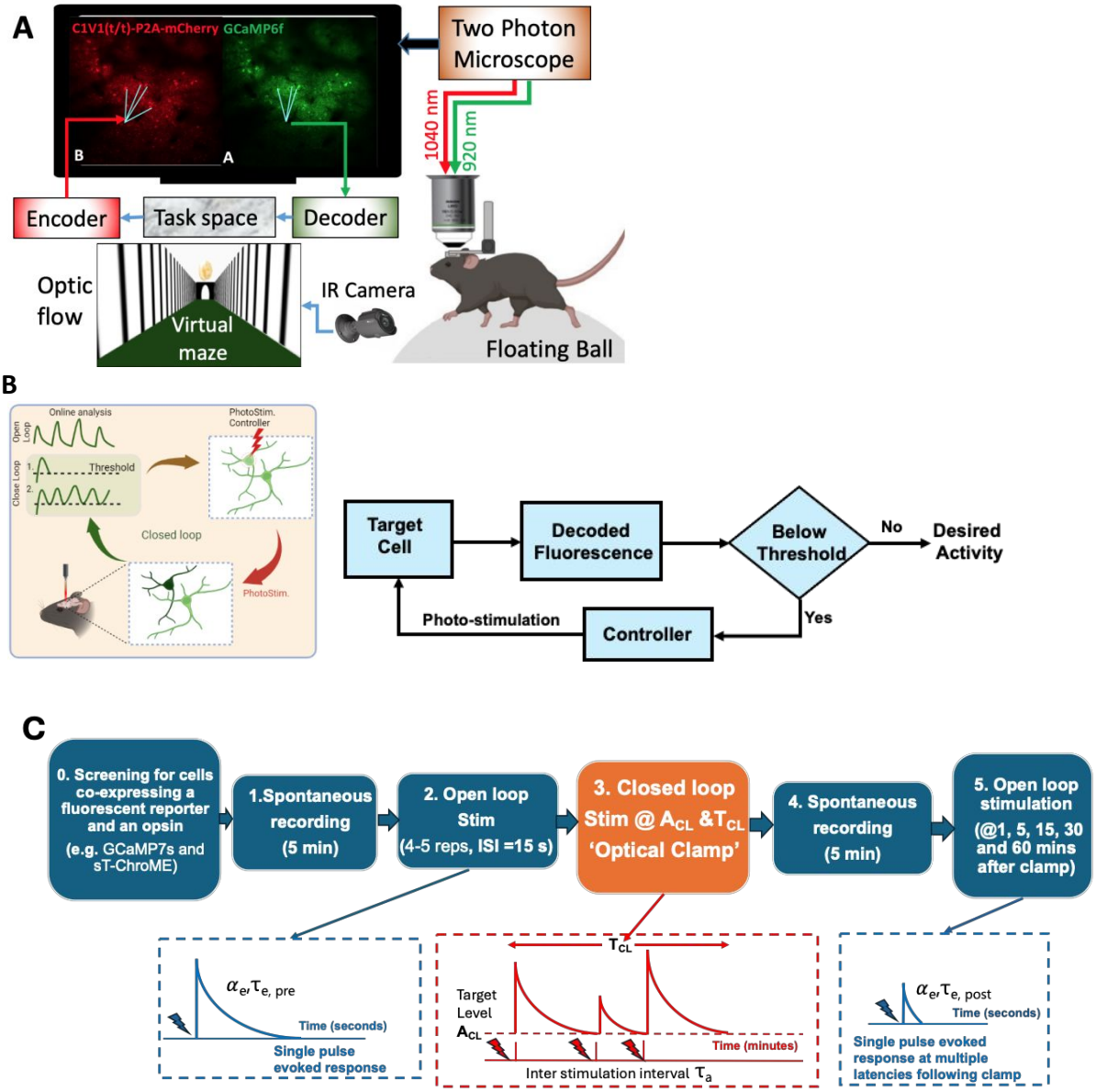

Figure 2

A. Schematic illustration of the experimental goal. A calcium sensor (e.g. GCaMP) generates an optical readout of neural activity, and an opsin (e.g. C1V1 or ChRmine) enables photostimulation. Exogenous BCI design uses the optical readout from one or more cells to actuate an end effector in the task space (e.g. cursor or virtual maze walls). Changes in the state of that end effector are then encoded in the pattern of photostimulation pulses delivered to target cells.

B. (Left) Endogenous BCI design bypasses the task space and directly photostimulates the same or different neurons based on the optical readout. (Right) Optical clamp approach: optical readout is decoded in real time and compared to a user specified target activity level either in the same cell or in other cells within the FOV.

C. Protocol for charactering BTSP and IP over a full experimental session. In the open loop step, each cell is photostimulated 4-5 times using a single pulse (50 ms, 5 spirals) separated by 15 seconds (for a total duration ~ 1 min) and the evoked Ca^{2+} traces are averaged to obtain a baseline for the global dendritic plateau potential before the optical clamp. This step is repeated at multiple time points following cessation of the clamp. The parameters α_e,τ_e are used to characterize the changes in the plateau potential observed in each case.

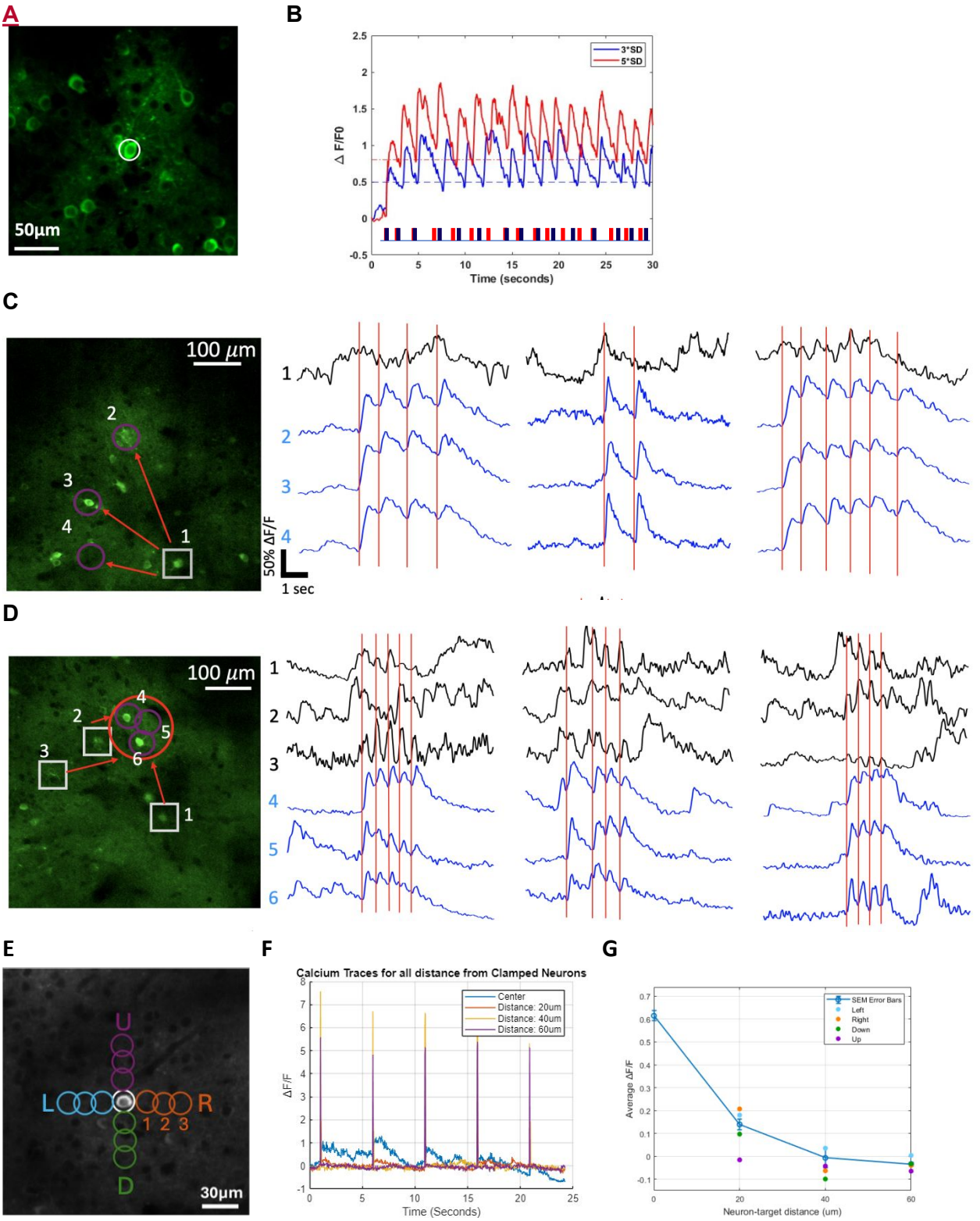
A
50µm
B
3*SD
5*SD
Δ F/F0
Time (seconds)
C
100 µm
1
2
3
4
50% ΔF/F
1 sec
D
100 µm
1
2
3
4
5
6
E
U
L
R
D
1 2 3
30µm
F
Calcium Traces for all distance from Clamped Neurons
Center
Distance: 20um
Distance: 40um
Distance: 60um
ΔF/F
Time (Seconds)
G
SEM Error Bars
Left
Right
Down
Up
Average ΔF/F
Neuron-target distance (um)

Figure 3.

A. Example field of view with a single neuron (white circle) co-expressing $ChRmine_{Kv2.1}$ and GCaMP7s targeted for closed loop poststimulation based on the protocol in Figure 2B.
B. Sample Ca^{2+} traces of the clamped neuron in A at two different target activity levels (mean + 3std and mean + 5std) for 30 sec. Ca^{2+} imaging was acquired at 30 Hz over a field of view of ~250 × 250 µm using a resonant galvo scanning system at 920 nm and photostimulated neurons via two-photon excitation at 1040 nm. The Spatial Light Modulator (SLM) generated a single photostimulation spot, which was scanned in a spiral fashion for 50 ms per pulse.
C. Examples of single and **D.** population input/output control. Grey square and traces are *trigger* neurons. Blue circles and traces are stimulated *target* neurons that are 'yoked' together. Red lines indicate stimulation trigger times conditioned on activity decoded from the trigger neurons.
E. A ~250 × 250 µm field of view demonstrating the stimulation spots used to verify off target effects.
F. Example Ca^{2+} traces from 'off center' color coded locations at 3 different spatial distances and 4 directions.
G. Ca^{2+} fluorescence decay profile at photostimulation spots 'off center' according to E and F.

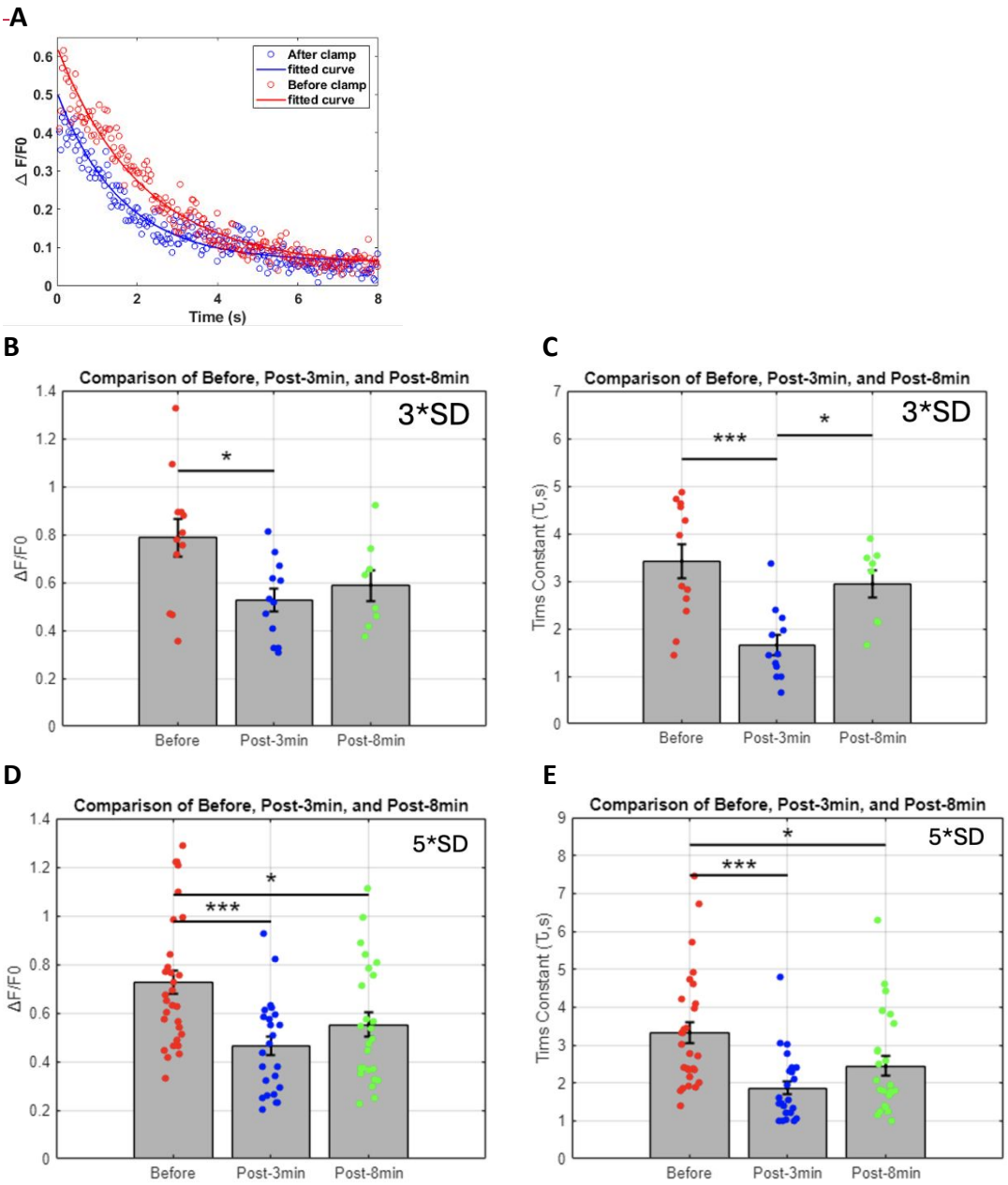

Figure 4:

A. Characterization of somatic Ca^{2+} response to open loop stimulation before and after clamp. Example average change in Ca^{2+} impulse response to single pulse open loop stimulation, a proxy of the plateau potential, before and after optical clamp at 5*standard deviation (5*SD) of baseline fluorescence for 200 seconds.

B. Changes in peak Ca^{2+} amplitude α_e following clamp at 3*SD target level (before vs post-3min: *p=0.011035) that partially rebounded at 8 mins (before vs post-8min: p=0.065906; post-3min vs post-8min: p=0.47326) (n=3 cells, N=3 mice).

C. Change in Ca^{2+} decay time constant τ_e following clamp at 3*SD target level (before vs post-3min:***p=0.00051785; before vs post-8min: p=0.31263; post-3min vs post-8min: *p=0.0032513) (n=3 cells, N=3 mice).

D. Changes in peak Ca^{2+} amplitude α_e following clamp at 5*SD target level (before vs post-3min: ***p= 0.00010167; before vs post-8min: *p=0.015294; post-3min vs post-8min: p=0.1656). (n=7 cells, N=3 mice).

E. Change in Ca^{2+} decay time constant τ_e following clamp at 5*SD target level (before vs post-3min: ***p=4.9042e-05; before vs post-8min: *p=0.024711; post-3min vs post-8min: p=0.076848). (n=7 cells, N=3 mice).

A **B**

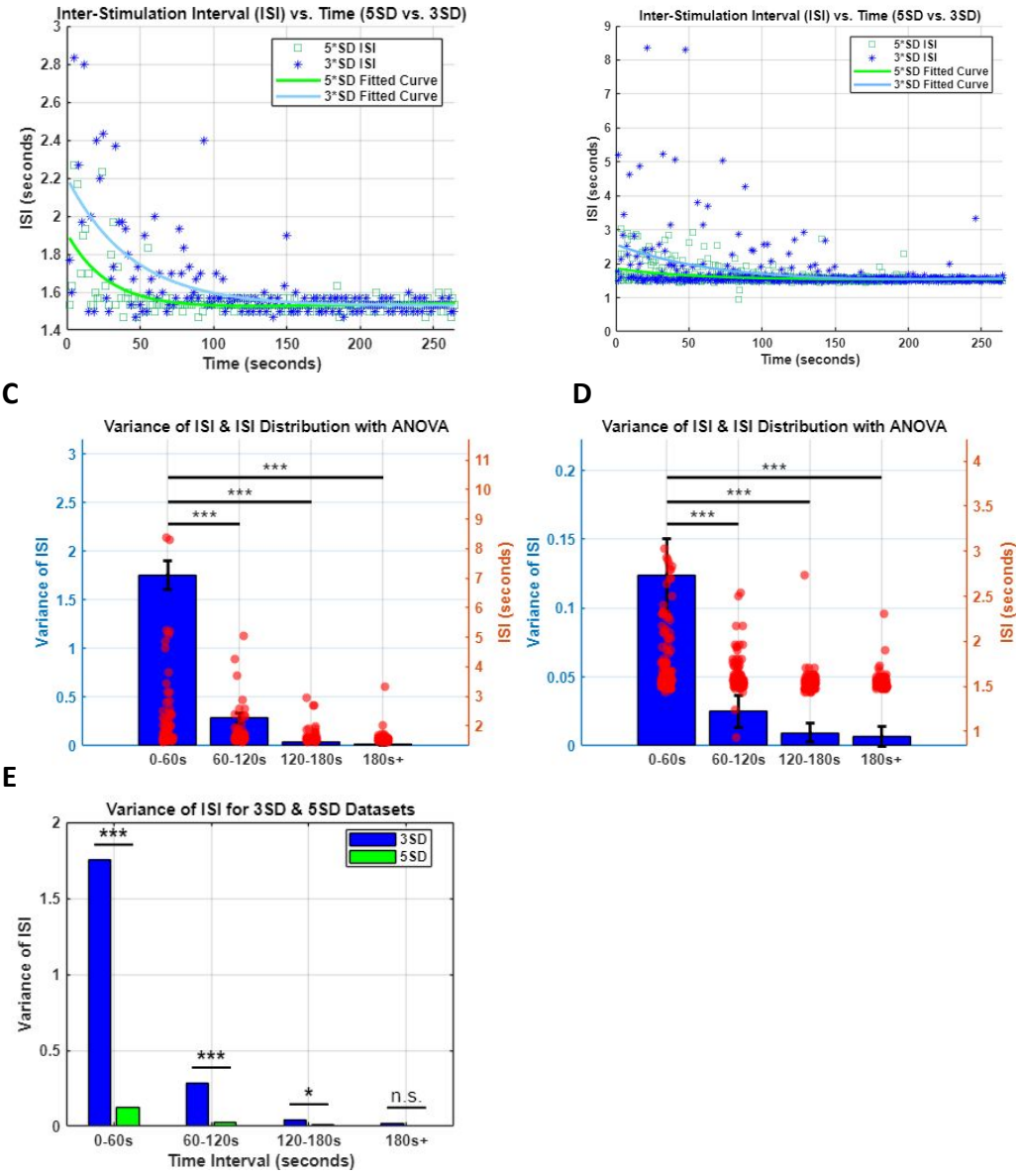

Figure 5:

A. Characterization of somatic Ca^{2+} response to closed loop stimulation. Example Inter Stimulation Interval (ISI) and exponential curve fitting associated with clamping one example cell at 3*SD and 5*SD.

B. Same as in A but for n=5 cells across N=4 mice.

C. ISI and its variance during clamp broken down by 60 seconds intervals for target activity level 3*SD. Optical parameters used are power= 10mW; 161 pulses per 266s (or 36 pulses/min). 0-60sec, 60-120sec:***p=9.50E-06; 0-60sec, 120-180sec:***p=6.68E-10; 0-60sec-180+:***p=1.25E-12; 60-120sec, 120-180sec:p=0.385; 60-120,180+:p=0.132; 120-180sec,180+: p=0.964.

D. Same as C but with target 5*SD resulting in 168 pulses per 266s (or 38 pulses/min).

[0-60sec, 60-120sec]:***p=2.13E-09; [0-60sec, 120-180sec]:***p=2.36E-15;[0-60sec-180+]:***p=4.37E-13; [60-120sec, 120-180sec]:p=0.266; [60-120,180+]:p=0.350; [120-180sec,180+]: p=0.99.

E. Comparison of ISI and its variance across two different levels across all cells in all mice (Two-Sample t test: Time interval 0-60s: ***p = 0.00003; 60-120s: ***p= 0.00074; 120-180s: *p= 0.01464; 180s+: p = 0.64271)

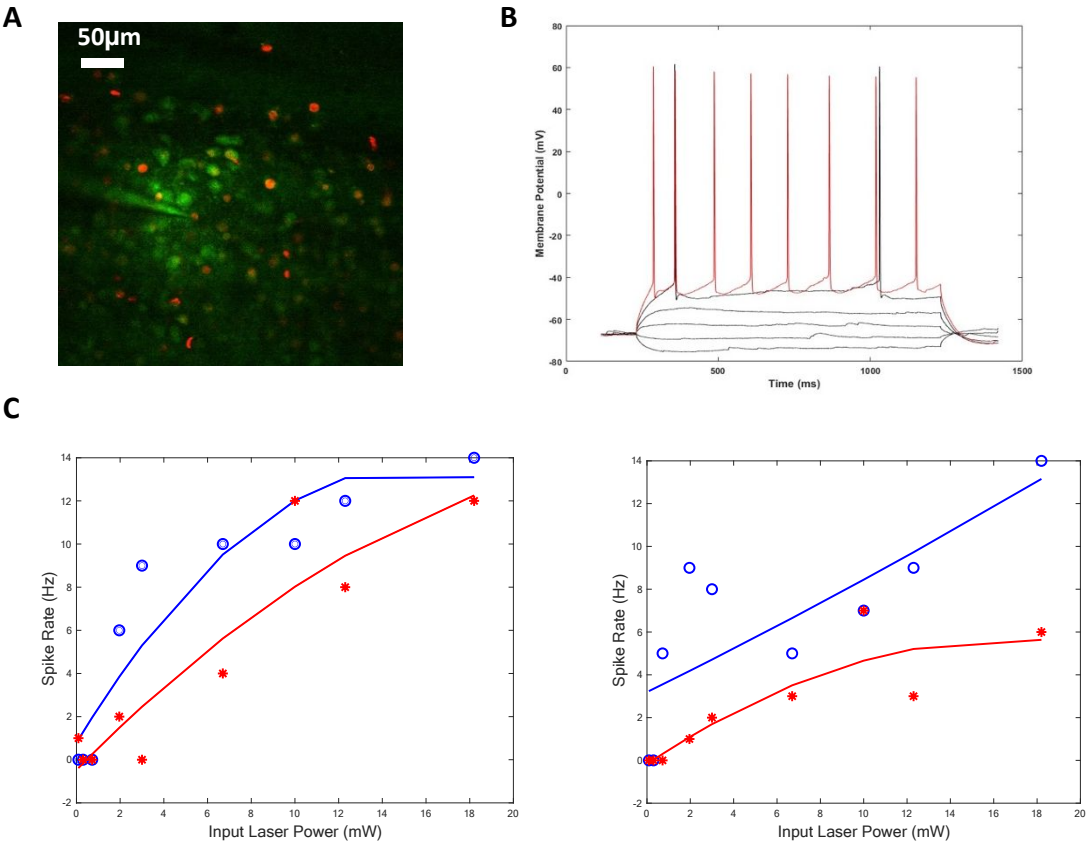

Figure 6

Characterization of changes in intrinsic excitability before and after optical clamp.

A. Representative field of view for two photon-guided whole-cell recording in current clamp mode to characterize the cell's f-I response.

B. Sample whole cell membrane voltage recordings to two depolarizing current levels (5uA black, 10 uA red) and multiple non-depolarizing current levels.

C. f-I characteristics before and after clamp (at 5*SD target level for 200 sec) for two example cells *in vivo*. Blue open circles and red asterisks represent input laser power (proxy for the current injected) to spike rate before and after clamp, respectively.

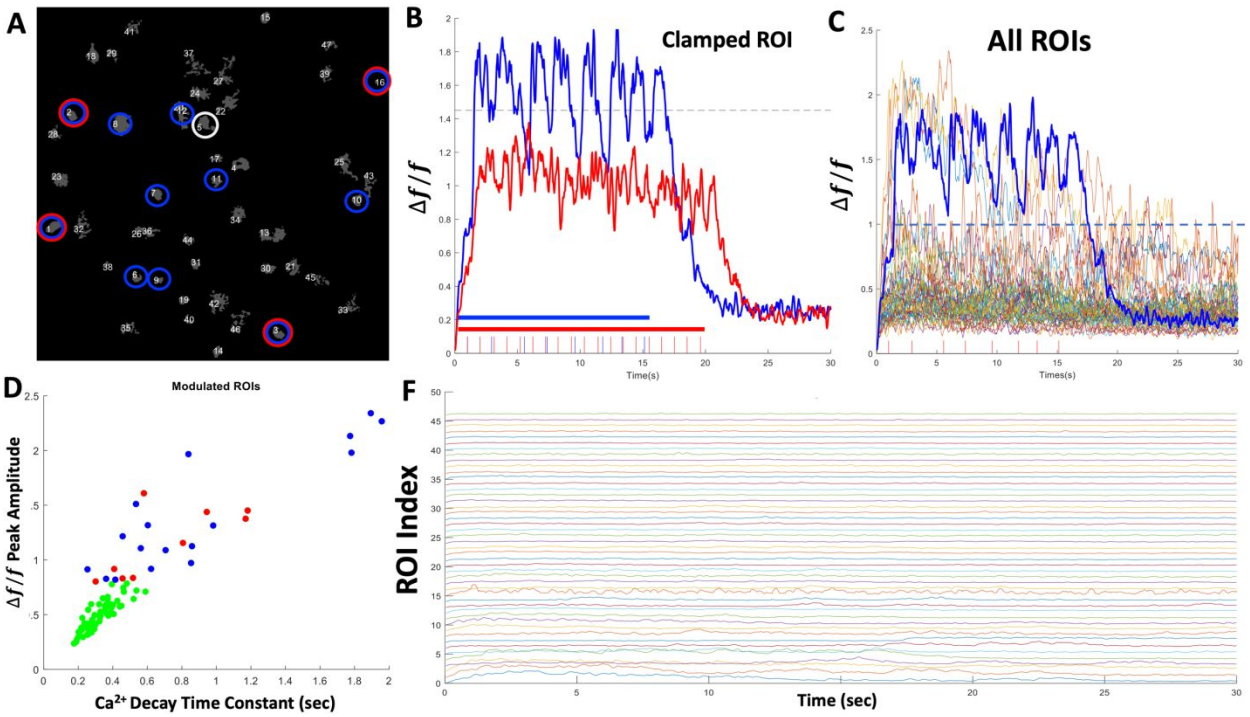

Figure 7

A. Example FOV containing 46 well isolated ROIs in mouse V1. ROI # 5 (circled in white) was selected for optical clamping at two target levels shown in B. ROIs circled in red are cell bodies showing significant increase in Ca^{2+} fluorescence intensity in response to target level (3*SD) in B. ROIs circled in blue are cell bodies showing significant increase in Ca^{2+} fluorescence intensity in response to clamp level (5*SD).

B. Activity of the clamped ROI#5 in A and photostimulation pulse trains used for each target level (red 3*SD, blue 5*SD).

C. Ca^{2+} fluorescence of all ROIs in the FOV during clamp interval for target 5*SD. ROIs showing significant modulation synchronized with the clamped ROI (n=17/46 cells, 5*SD target, **p = 0.0011) correspond to blue circled ROIs in A.

D. Ca^{2+} peak fluorescence versus Decay Time constant for all 46 ROIs in the FOV for target level 5*SD in C. Each dot represents the average of Ca^{2+} peak fluorescence and event decay time constant locked to each photostimulation pulse during the clamp. Green dots are ROIs that were not significantly modulated within the clamp period (n=29;p=0.152).

F. Raw Ca^{2+} fluorescence for all 46 ROIs in A at target 5*SD. Significantly modulated ROIs are plotted consecutively to demonstrate the difference between the activated and non-activated ROIs shown in C following cessation of the clamp at 15 sec.

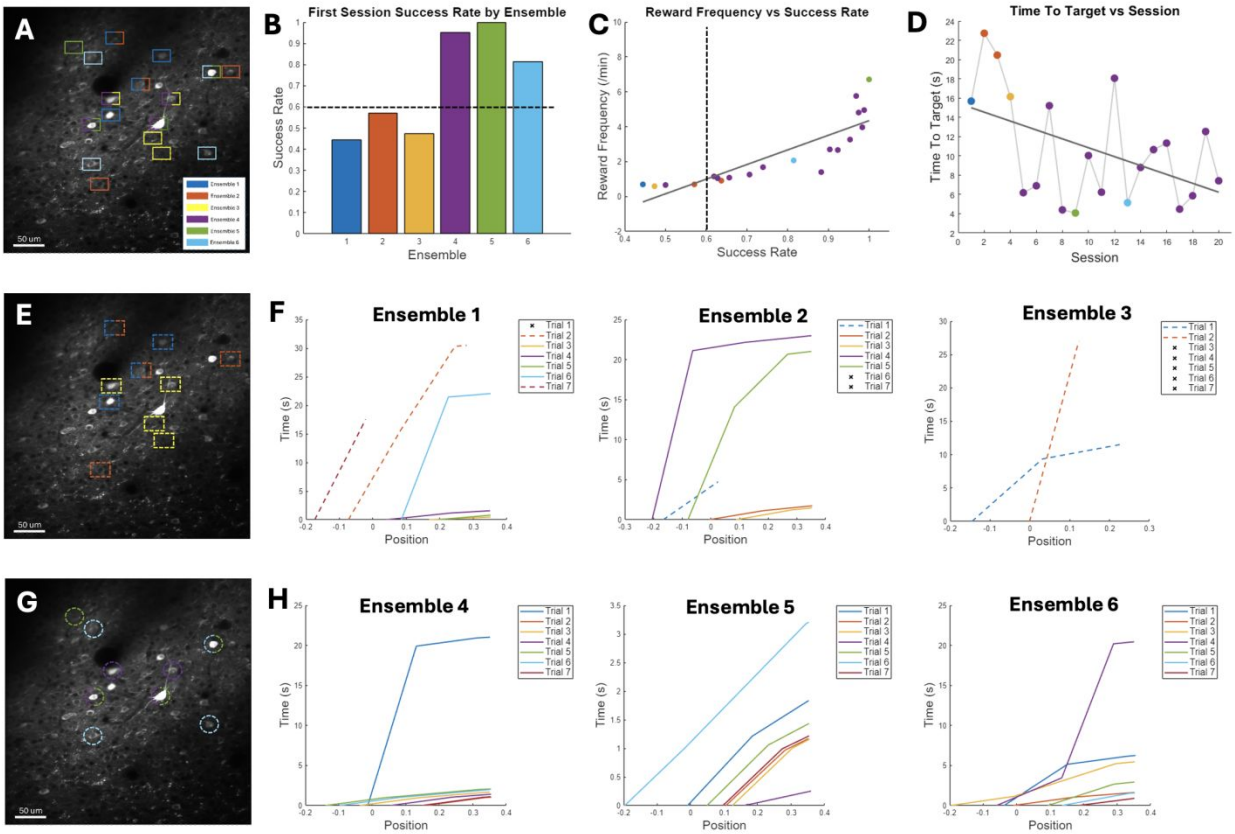

Figure 8

A. Field of View where six different ensembles of 4 neurons each were used to train the animal on the BCI task over 6 different sessions. Some ensembles overlapped whereas others did not.

B. Success rate in the first session for each of the ensembles in A. Dashed line indicate a threshold of 60% success that was used to categorize the ensembles into either a 'weak/slow learner' (E1-E3) or a 'strong/rapid learner" ensemble (E4-E6).

C. Average Time to Target in each session (color coded by ensemble) demonstrating continuous decrease over sessions for E4.

D. Time to Target over sessions for E4 and for session 1 of the other 5 ensembles. Strong learner E4-6 exhibited a TT= 6.21+ 6.1 sec over 20 sessions compared to TT= 17.8 + 20.2 sec for the weak learner ensemble category.

E. Same FOV as A but highlighting only the neurons selected for ensembles 1-3 using the same color code in A.

F. Cursor path from initial start position to target position in the first 7 trials of the first session for ensembles 1-3. Dashed lines indicate incomplete trial, whereas x indicates a failed trial (timeout).

G. Same FOV as A but highlighting only the neurons selected for ensembles 1-3 using the same color code in A.

H. Cursor path from initial start position to target position in the first 7 trials of the first session for ensembles 4-6.

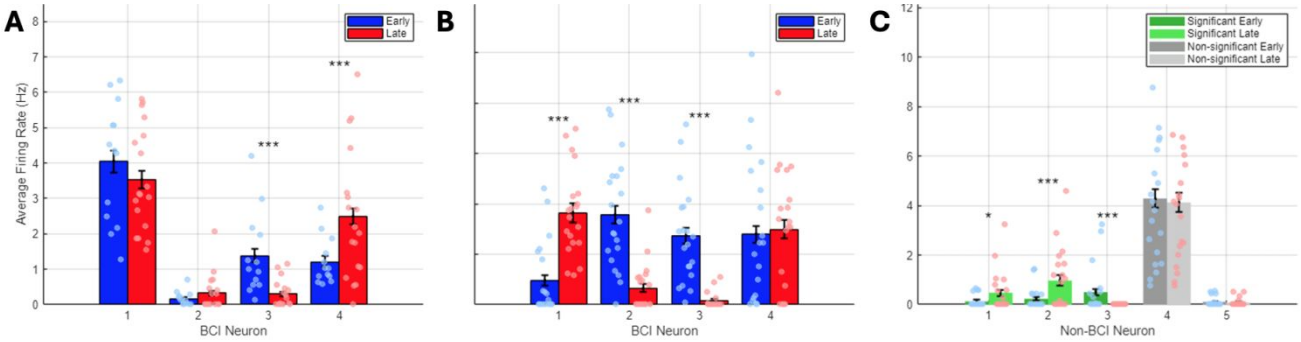

Figure 9:

A. Average firing rate of BCI neurons during BCI control in the same ensemble (E4) comparing an early session versus a later session (2 weeks apart). Each dot represents the average firing rate over a 50 second interval within ~10 mins of behavioural trials. Success rate in both sessions was 90% and 98%, respectively.

B. Baseline firing rate comparison for the same ensemble in **A** outside of behavior. Each dot represents the average firing rate over a 50 second interval within ~8 mins.

C. Baseline firing rate of non-BCI neurons in the same sessions as A. Each dot represents the average firing rate over a 50 sec interval within ~8 mins (p=0.013;0.00085;3.77e-05;0.756;0.598 for neurons 1-5 respectively, two-sided t-test)